Charge Carrier Mobility, Photovoltaic, and Electroluminescent Properties of Anthracene-Based Conjugated Polymers Bearing Randomly Distributed Side Chains

Özlem Usluer,[1,2] Christian Kästner,[3] Mamatimin Abbas,[1,4] Christoph Ulbricht,[1] Vera Cimrova,[5] Andreas Wild,[6] Eckhard Birckner,[7] Nalan Tekin,[8] Niyazi Serdar Sariciftci,[1] Harald Hoppe,[3] Silke Rathgeber,[9] Daniel A. M. Egbe[1]

[1]Linz Institute for Organic Solar Cells, Physical Chemistry, Johannes Kepler University Linz, Altenbergerstr. 69, 4040 Linz, Austria
[2]Department of Chemistry, Mugla University, Kotekli, 48000 Mugla, Turkey
[3]Institute of Physics, Ilmenau University of Technology, Weimarer-Str. 32, 98693 Ilmenau, Germany
[4]Laboratoire IMS,Université Bordeaux 1, UMR 5218 CNRS, ENSCBP, 16 Avenue Pey-Berland, 33607 Pessac Cedex, France
[5]Institute of Macromolecular Chemistry, Academy of Sciences of the Czech Republic, Heyrovský Sq. 2, 16206 Prague 6, Czech Republic
[6]Institute for Organic Chemistry and Makromolecular Chemistry, Friedrich-Schiller University Jena, Humboldtstr. 10, 07743 Jena, Germany
[7]Institute of Physical Chemistry, Friedrich-Schiller University Jena, Lessingstr. 10, 07743 Jena, Germany
[8]Department of Chemistry, Kocaeli University, Umuttepe, 41380 Kocaeli, Turkey
[9]Institut für Integrierte Naturwissenschaften, Universität Koblenz-Landau, Universitätsstr. 1, 56070 Koblenz, Germany
Correspondence to: D. A. M. Egbe (E-mail: daniel_ayuk_mbi.egbe@jku.at)

Received 28 February 2012; accepted 18 April 2012; published online 25 May 2012
DOI: 10.1002/pola.26133

ABSTRACT: This article reports on the synthesis, characterization, and properties of various anthracene-containing poly(*p*-phenylene-ethynylene)-*alt*-poly(*p*-phenylene-vinylene) (PPE-PPV) polymers (AnE-PVs) bearing statistical distributions of various side chains. Primarily, the ratio of linear octyloxy and branched 2-ethylhexyloxy side chains at the poly(*p*-phenylene vinylene) (PPV) parts was varied, leading to the polymers *stat*, *stat*1, and *stat*2. Furthermore, polymers also containing asymmetric substituted PPV and poly(*p*-phenylene ethynylene) units (bearing methoxy and 2-ethylhexyloxy side chains) were prepared yielding *stat*3, *stat*4, and *stat*5. These materials exhibit a broad variation in their photovoltaic properties. It is once more shown that side chains and their distribution can crucially affect the photovoltaic device performance. The introduction of units with asymmetric substitution into these systems seems to be harmful for their utilization in photovoltaic applications. Organic field-effect transistors were fabricated to investigate hole mobilities in these new materials. Large variance was observed, falling in the range of almost two orders of magnitude, indicating rather different π–π stacking behavior of the polymer backbones owing to side-chain modifications. Moreover, a selection of the new polymeric systems was investigated regarding their potential for light-emitting diode (LED) applications. Polymer LEDs using the polymers AnE-PV*stat*, -*stat3*, -*stat4*, and -*stat5*, as the active layer showed turn-on voltage of $\sim$2 V and exhibited red light emission. © 2012 Wiley Periodicals, Inc. J Polym Sci Part A: Polym Chem 50: 3425–3436, 2012

KEYWORDS: conjugated polymers; organic field-effect transistors; organic solar cells; light-emitting diodes; photophysics

INTRODUCTION Conjugated polymer-based organic photovoltaic (OPV) devices are highly promising for the realization of low-cost solar cells and are therefore of high research interest since the last two decades.[1–5] Worldwide interdisciplinary investigations result in a rapid improvement of the power conversion efficiency (under AM1.5 illumination, $\eta_{AM1.5}$). Certified $\eta_{AM1.5}$ values above 7% have been reported recently for polymer based OPVs.[6] Organic solar cells with 10.0% efficiency (unstabilized) were reported by Mitsubishi Chemical in 2011.[7] First OPV-based products are commercially available.[8] The bulk heterojunction concept involving the intermixing of donor and acceptor components in the active layer has been proven to be the most efficient way to design high-performance devices, up to now. Different approaches to tune the nanoscale morphology of the solar cell active layer, leading to improvement of the final device performance have been reported.[9]

Previous studies on poly(*p*-phenylene-ethynylene)-*alt*-poly(*p*-phenylene-vinylene)s (PPE-PPVs) have shown that solubilizing alkoxy side chains can also be utilized to affect the active layer blend morphology of PPE-PPV/fullerene bulk heterojunctions. By varying the mole fractions of units with different side-chain species, the photovoltaic properties can be optimized.[10,11] It has been demonstrated that linear and branched alkoxy side groups and combinations thereof can be used to vary the backbone π–π-stacking distance ($d_{\pi-\pi}$) and the interlayer separation (d_{inter}) of anthracene-containing PPE-PPVs. The photovoltaic properties could be optimized by random distribution of linear and branched side chains at the PPE and PPV sections of the copolymers, leading to power conversion efficiencies of around 4%, the highest values so far reported for PPV-based materials.[12] Encouraged by these findings, our focus was directed on the effect of statistical distribution of side chains on the photovoltaic response of AnE-PVs.

Electroluminescent (EL)-conjugated polymers are used in flat panel display due to their beneficial properties. Good processability and flexibility go together with low operating voltages, fast response times, and facile color tunability over the full visible range. A broad variety of light-emitting polymers such as poly(*p*-phenylene vinylene)s (PPVs),[13–18] polythiophenes,[19] poly(*p*-phenylene)s,[20] carbazole-containing polymers,[21] and polyfluorenes[22,23] as well as combinations thereof have been reported. PPV and its derivatives are known as promising materials for polymer light-emitting diodes (PLEDs) owing to their relatively high photoluminescence (PL)[24] and EL quantum efficiencies as well as their good mechanical strength, thermal stability, and the possibility to vary the color by changing the substituents at the aromatic ring. Functionalization of PPV with alkoxy groups reduces the energy bandgap, leading to a distinct red-shift in emission.[25] Poly(*p*-phenylene ethynylene)s (PPEs) are another interesting class of conjugated polymers. The highly rigid systems possess high fluorescence quantum yields. The emission color of PPEs can be tuned by the incorporation of other arylene-building blocks during the polymerization process. Red EL can be obtained from copolymers with anthracene[26,27] or benzothiadiazole[28] units. Anthracene-containing polymers have been used as organic optoelectronic materials due to their high fluorescence quantum yields.[29] Anthracene is very appealing as building block. The rigid structure can be easily functionalized at its ninth and 10th position and demonstrate high thermal stability and high device stability.[30]

This report describes the synthesis and characterization of a number of anthracene-containing PPE-PPVs bearing various side-chain combinations and distributions. The molecular masses of the polymers were estimated by gel permeation chromatography (GPC). The photophysical properties were investigated by UV–vis absorption and PL measurements in dilute chlorobenzene solution as well as in thin film. The electrochemical behavior of the polymers was investigated by cyclic voltammetry (CV). Differential scanning calorimetry (DSC) and thermogravimetric analysis (TGA) were used to study the thermal behavior of the materials. Detailed investigations regarding charge carrier mobility and potential for photovoltaic and light-emitting applications were conducted.

EXPERIMENTAL

All reagents and solvents were purchased from Aldrich and used without further purification. Alq_3 and Poly(3,4-ethylenedioxythiophene) poly(styrenesulfonate) (PEDOT:PSS) (Baytron/Clevios PH HCE 10P301) for EL device fabrication were also obtained from Aldrich and HC Starck, respectively. Indium tin oxide (ITO)-covered glass plates were supplied by Kintec (China).

The measurements of size exclusion chromatography were conducted on a Viscothek HT-GPC instrument with two PLgel-mixed bead columns assembled in series and a refractive index detector. Tetrahydrofuran (THF) containing 0.1% (w/w) tetra-*n*-butyl ammonium nitrate was applied as eleutent at a temperature setting of 35 °C. A calibration with polystyrene (PS) standards was used to estimate the molecular data of the polymers. A Perkin-Elmer Pyris 6 thermal analyzer was used for TGA experiments.

DSC measurements were performed on a Mettler DSC 822 applying a nitrogen-purged cell. For the calibration of the temperature and enthalpy changes, an indium standard was used.

Wide-angle X-ray scattering (WAXS) experiments in transmission geometry were carried out at a wavelength of $\lambda = 0.154$ nm (CuKα radiation). A two-pinhole collimation system provides a beam of about 0.5 mm in diameter. The diffraction patterns were recorded with a collection time of 1 h on a two-dimensional (2D) area detector (Image plate Mar345, Ø 345 mm, pixel size 100 μm^2). The 2D data are corrected for background scattering from the quartz capillary and subsequently radially averaged. The detector distance was determined by means of a silver behenate standard.

CV was used to study redox properties. The ionization potential (HOMO level), E_{IP}, and electron affinity (LUMO level), E_A, were estimated from the onset potentials E_{onset} based on the reference energy level of ferrocene (4.8 eV below the vacuum level) using the equation E_{IP} (E_A) = $-(E_{onset} - E_{ferr}) - 4.8$ (eV), where E_{ferr} is the value for ferrocene versus the Ag/Ag^+ electrode. The E_{IP} and E_A values were evaluated as the average from CV curves measured on several samples at scan rates of 50 mV s^{-1}.

Thin-film PL spectra were measured using a home-built PL setup. Thin-film absorption spectra were recorded on a Varian Cary 5000 UV/vis spectrophotometer. Topography measurements were performed with a Veeco Nanoscope atomic force microscope (AFM) in tapping mode. Thin films were spin cast on glass substrates from chlorobenzene solutions. Solar cell device preparation involved the etching of the ITO-covered glass substrates for selective contacting of the back electrode, followed by spin-coating of PEDOT:PSS. The photoactive layer was deposited by spin-casting solutions of AnE-PV/[6,6]-phenyl-C_{61}-butyric acid methyl ester (PCBM) (1:2) with 0.75 wt % of the polymer. For the top electrodes, aluminum was evaporated by vacuum deposition. Current–

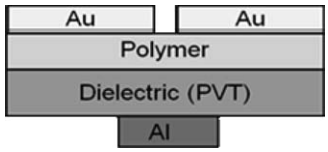

FIGURE 1 Bottom gate, top-contact (staggering) field-effect transistor device structure used in this work.

voltage (*I–V*) curves were recorded with a Keithley 2400 source-measure-unit irradiating the solar cell devices (0.5-cm^2 active area) with a class A AM1.5 solar spectrum simulator. External quantum efficiency (EQE) measurements were conducted with a Bentham PVE300 photovoltaic spectral response characterization system. Thin films prepared for optical investigation and solar cell devices were not annealed.

Bottom gate, top-contact organic field-effect transistor (OFET) devices were fabricated. The schematic structure is drawn in Figure 1. Water soluble poly(1-vinyl-1,2,4-triazole) (PVT) was chosen as the dielectric, as it was shown to give low leakage current and low trap densities in our previous studies.[31] PVT was dissolved in high-resistant ultrapure water in a weight ratio of 7%. The solution was filtered and spin-coated on glass substrate with thermally evaporated Al gate contact. The films were dried in a vacuum oven overnight at a temperature of 50 °C. Capacitance was about 5 nF cm^{-2}. The polymers (AnE-PVs) were dissolved in chlorobenzene (10 mg mL^{-1}) and spin-coated (1500 rpm for 40 s and 2000 rpm for 20 s) directly on top of PVT in a nitrogen atmosphere glove box. The films were kept within the glove box overnight and annealed at 100 °C for 5 min to remove traces of solvents. Gold source/drain contacts were evaporated thermally through shadow mask to complete the OFET devices. Devices were further annealed at 100 °C for 10 min to decrease the contact resistance between polymers and the source/drain contacts. Channel length is 0.05 mm and channel width is 3.0 mm. *I–V* characterizations were performed using Agilent E5273A in nitrogen glove box.

For PLED preparation, ITO glass substrate with a sheet resistance of 15 Ω/□ was used. After etching ITO and cleaning in an ultrasonic bath with acetone and isopropanol according to standard cleaning procedure, the active area with 10 mm^2 was obtained. PEDOT:PSS was spin-coated onto the substrate at a spin speed of 4000 rpm for 30 s forming 50-nm thick layers. The samples were annealed under nitrogen atmosphere for 30 min at 150 °C. Chlorobenzene solutions of polymer (1%, w/v) were spin-coated onto the ITO at a spin speed of 1500 rpm for 30 s to get 80 nm thick layers. Finally, an ultrathin LiF layer (0.5 nm) and Al cathode (100 nm) were evaporated under high vacuum by using a shadow mask. The characterization of the fabricated devices was carried out under inert nitrogen environment inside a glove-box system. A Keithley 236 source meter was used to investigate *I–V* characteristics. The EL and luminance properties were measured using a Spectrascan PR-655 spectroradiometer. The thicknesses of films were determined with a Digital Instrument 3100 AFM.

RESULTS AND DISCUSSION

The synthesis of the PPE-PPV polymers (AnE-PV*stat, stat1-5*) was conducted following a well established procedure which uses the Horner–Wadsworth–Emmons olefination reaction to polycondensate dialdehydes and bisphosphonate esters (Scheme 1).[10,32] While the ethynyl motifs are already embedded in the applied dialdehydes, the vinylene features are formed on polycondensation. By reacting the anthracene-based dialdehydes (1a, 1b, and/or 1c) with the phenyl-based bisphosphonate esters (2a, 2b, and/or 2c), which only vary in their attached side chains—1a/2a octyloxy (linear chains), 1b/2b 2-ethylhexyloxy (branched chains), 1c/2c methoxy and 2-ethylhexyloxy (asymmetric substituted units), and polymers with an identical conjugated backbone, but diverse combinations and distributions of side chains were realized (AnE-PV*stat, stat1-5*). The selected monomers combined statistically according to the applied ratios to form the polymers AnE-PV*stat* ($1a_{(1)}1b_{(1)}2a_{(1)}2b_{(1)}$), AnE-PV*stat1* ($1a_{(1)}1b_{(1)}2a_{(2)}$), and AnE-PV*stat2* ($1a_{(1)}1b_{(1)}2b_{(2)}$) with linear (octyloxy) and branched (2-ethylhexyloxy) side chains as well as AnE-PV*stat3* ($1b_{(1)}1c_{(1)}2b_{(1)}2c_{(1)}$), AnE-PV*stat4* ($1a_{(1)}1c_{(1)}2a_{(1)}2c_{(1)}$), and AnE-PV*stat5* ($1a_{(1)}1b_{(1)}1c_{(1)}2a_{(1)}2b_{(1)}2c_{(1)}$), which furthermore contain unsymmetrically substituted units (methoxy and 2-ethylhexyloxy side chains). The final products were obtained with yields between 60 and 80% after extraction of the raw materials with a hot mixture of diethyl ether and methanol. All

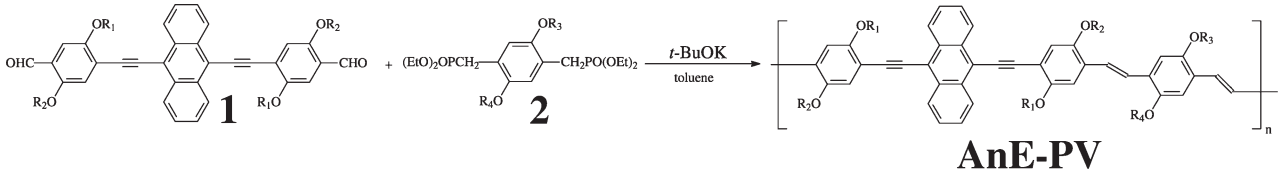

1a, **2a**: $R_1 = R_2 = R_3 = R_4$ = octyl. **1b**, **2b**: $R_1 = R_2 = R_3 = R_4$ = 2-ethylhexyl. **1c**, **2c**: $R_1 = R_3$ = methyl, $R_2 = R_4$ = 2-ethylhexyl

1a$_{(1)}$ + **1b**$_{(1)}$ + **2a**$_{(1)}$ + **2b**$_{(1)}$ ⟶ **AnE-PV*stat***

1a$_{(1)}$ + **1b**$_{(1)}$ + **2a**$_{(2)}$ ⟶ **AnE-PV*stat1***

1a$_{(1)}$ + **1b**$_{(1)}$ + **2b**$_{(2)}$ ⟶ **AnE-PV*stat2***

1b$_{(1)}$ + **1c**$_{(1)}$ + **2b**$_{(1)}$ + **2c**$_{(1)}$ ⟶ **AnE-PV*stat3***

1a$_{(1)}$ + **1c**$_{(1)}$ + **2a**$_{(1)}$ + **2c**$_{(1)}$ ⟶ **AnE-PV*stat4***

1a$_{(1)}$ + **1b**$_{(1)}$ + **1c**$_{(1)}$ + **2a**$_{(1)}$ + **2b**$_{(1)}$ + **2c**$_{(1)}$ ⟶ **AnE-PV*stat5***

SCHEME 1 Synthesis of anthracene-based PPE-PPVs with statistical distribution of side chains.

TABLE 1 The Monomer Composition, GPC Data, Yields, and TGA Results of the Statistical Copolymers AnE-PV

AnE-PV	1a	1b	1c	2a	2b	2c	M_n (g mol^{-1})	PDI	Yield (%)	$T_{5\%}$ (°C)	$T_{10\%}$ (°C)
-stat	1	1	0	1	1	0	6,600	4.0	80	312	321
-stat1	1	1	0	2	0	0	68,400	1.99	61	326	375
-stat2	1	1	0	0	2	0	11,500	2.27	94	328	360
-stat3	0	1	1	0	1	1	3,700	5.3	72	351	379
-stat4	1	0	1	1	0	1	9,100	3.3	70	334	370
-stat5	1	1	1	1	1	1	7,500	4.0	60	344	371

synthesized polymers are soluble in common organic solvents such as chloroform, dichloromethane, THF, toluene, and chlorobenzene. Results obtained from GPC measurements as well as yields of the materials are provided in Table 1.

Structural and Thermal Properties

TGA measurements were performed in ambient atmosphere at a heating rate of 10 K min^{-1}. Figure 2 presents the corresponding TGA curves (mass M as a function of the temperature normalized to initial mass M_0 at room temperature) of all samples. The decomposition temperatures listed in Table 1 were taken at 5 and 10% weight loss, respectively. The results indicate decomposition well above 300 °C for all synthesized polymers.

Samples of the synthesized polymers were investigated with DSC in nitrogen atmosphere. To check for thermal transitions, the temperature range from 25 to 250 °C was scanned at a heating/cooling rate of 10 K min^{-1}. Each sample underwent in total two heating–cooling cycles. In Figure 3, the enthalpy changes recorded during the first heating runs are presented as a function of temperature. No transitions are visible in the subsequent heating and cooling cycles. Apparently, the transitions that are only occurring in the first heating run result from nonequilibrium structures frozen-in during preparation process. Thin-film deposition by spin-coating also leads to frozen-in nonequilibrium structures. Thus, the DSC measurements can give important insight into proper annealing procedures. The transitions temperatures determined at the peak maxima are included in Figure 3.

The as-prepared samples (powders) all show an endothermic transition at low temperatures (50–65 °C). These solid–solid transitions are presumed to originate from an order–disorder transition (melting) of the side chains. Because of the absence of the low-temperature transition in the subsequent

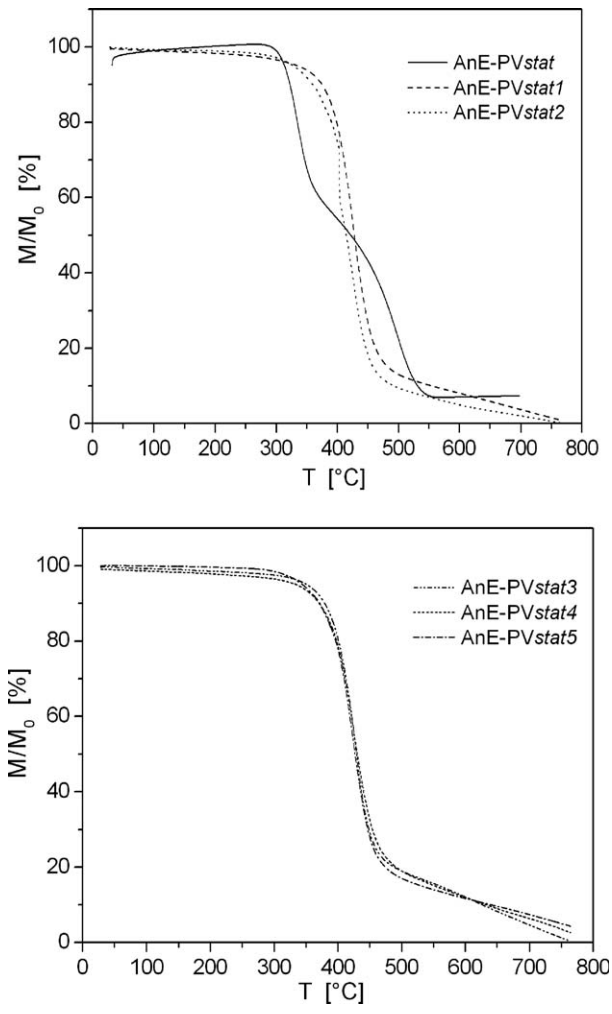

FIGURE 2 TGA diagrams of AnE-PV*stat,- stat1,- stat2,- stat3,- stat4,* and *–stat5*.

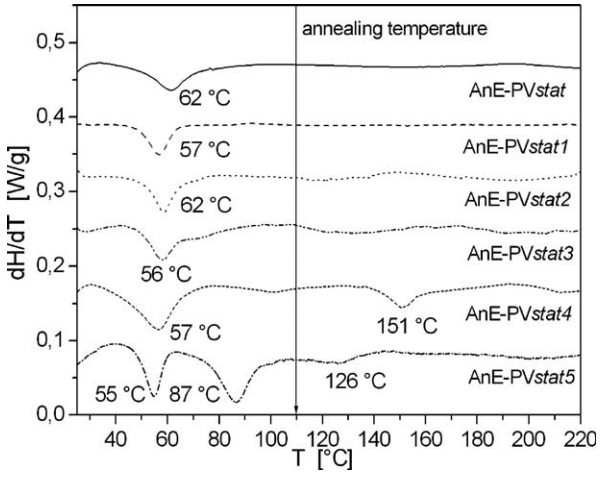

FIGURE 3 DSC results of AnE-PV*stat,- stat1,- stat2,- stat3,- stat4,* and *-stat5*: first heating runs.

runs, the side chains are most likely amorphous in the equilibrium structure.

For further structural investigation, WAXS experiments were conducted. Figure 4 shows the averaged data as a function of the norm of the scattering vector $q = 4\pi/\lambda \sin(2\theta)$, where 2θ is the scattering angle. Data are shifted in intensity for clarity.

The WAXS results show that only the symmetric substituted polymer AnE-PV*stat* carrying equal amounts of linear and branched side chains exhibits longer ranged order. Annealing of the polymer at 110 °C, above the side-chain melting temperature, somewhat improves the degree of order. The symmetric substituted polymers carrying an increased percentage of linear or branched side chains, AnE-PV*stat1* and AnE-PV*stat2*, are amorphous. Annealing at 110 °C does not improve the degree of order in these cases.

Asymmetric functionalization with side chains also results in amorphous polymers. For the polymer carrying branched side chains only (in symmetric and asymmetric conformation), in the DSC thermograms, only the side-chain melting transition is observed. Annealing does not improve the degree of order. For the samples with (partly) octyloxy substituents, AnE-PV*stat4* and AnE-PV*stat5*, beside the side-chain melting transition, additional endothermic solid–solid transitions are observed at higher temperatures (Fig. 3). The polymer AnE-PV*stat4*, linear, symmetric, and branched, asymmetric functionalized with side chains shows an extra transition at 151 °C. For the polymer AnE-PV*stat5* comprising of building blocks with both branched and linear, symmetric, as well as branched, asymmetric substituents two more transitions at 87 and 126 °C are observed.

Annealing of these polymers (AnE-PV*stat4* and *5*) leads to a shift of the first peak to smaller q values, that is, smaller inter-backbone distances. For the polymer AnE-PV*stat5*, the annealing temperature lies above the transitions temperature of one of the high-temperature transitions. The WAXS results obtained for this polymer indicate some crystallinity in the annealed sample. Obviously, these high-temperature transitions involve structure changes in the samples that give the backbones some degree of flexibility to reorganize when cooled back to room temperature.

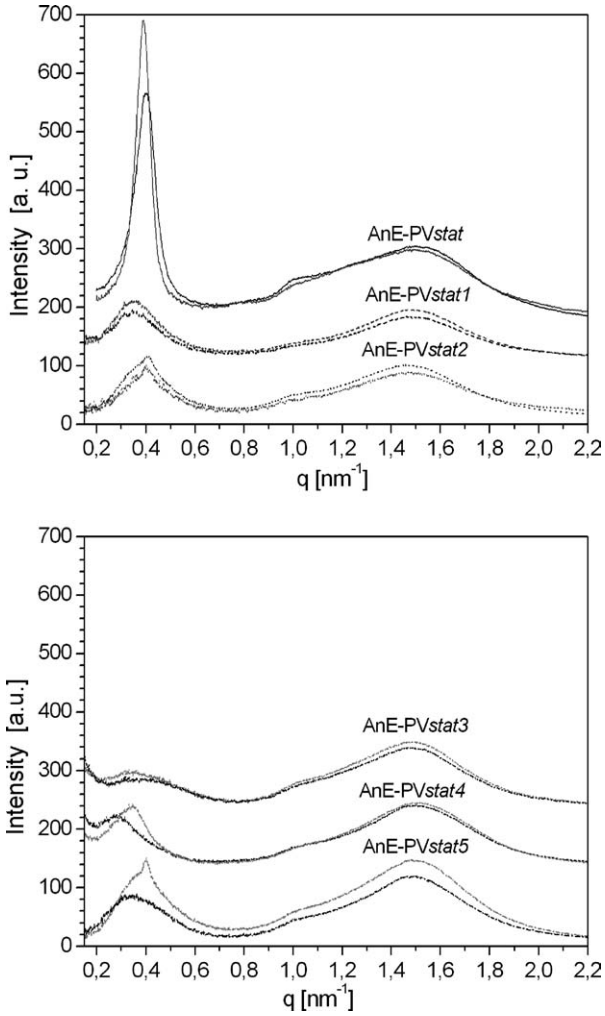

FIGURE 4 WAXS spectra of AnE-PV*stat,- stat1,- stat2,- stat3,- stat4,* and -*stat5*: materials as synthesized (dark) and annealed (110 °C, pale) samples.

Photophysical Investigations

The absorption and emission spectra of AnE-PV*stat,- stat1,- stat2,- stat3,- stat4*, and -*stat5* in solution and in thin film are shown in Figure 5. Tables 2 and 3 summarize the photophysical data. In solution, the AnE-PVs absorb around 500 nm and show fluorescence with maxima (λ_f) around 580 nm.

Upon closer inspection, the polymers can be classified in three groups. The polymers with absorption maxima (λ_a) between 500 and 515 nm have almost identical fluorescence spectra ($\lambda_f \approx 582$ nm) and fluorescence quantum yields, Φ_f, between 10 and 20% (AnE-PV*stat1, 2, 4, 5*).

AnE-PV*stat3* is the only polymer that possesses an absorption maximum below 500 nm (491 nm) in solution and exhibits a significantly broad emission spectrum with the lowest Φ_f value of 3%. We explain this with the least coplanarized polymer backbone due to the largest number of bulky 2-ethyl hexyl side chains close to the anthracene moieties.

AnE-PV*stat* has the most stabilized and coplanarized conjugated system, which is reflected by the red-shift of absorption, the smallest Stokes shift (960 cm^{-1}) and smallest full-width-at-half-maximum (FWHM) of fluorescence spectrum (1100 cm^{-1}), the highest fluorescence quantum yield, and the smallest nonradiative deactivation constant, k_{nr} (Table 2).

All the polymers show complex but wavelength-independent fluorescence kinetics, which cannot be attributed to polarization effects (measurements under magic angle). The evaluation requires a biexponential calculation model for AnE-PV*stat* and a triexponential for the others. The mean lifetimes ($<\tau>$) given in the tables correlate well with the Φ_f-values. This correlation in combination with almost identical fluorescence spectra is an indication of a similar fluorescent S_1 state.

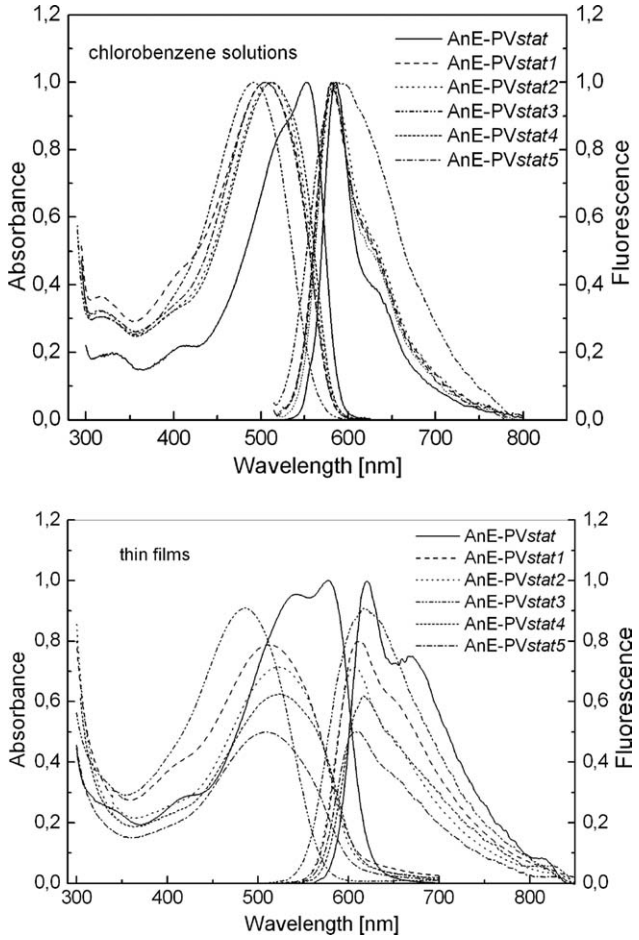

FIGURE 5 Absorption and emission spectra of AnE-PV*stat,- stat1,- stat2,- stat3,- stat4,* and *-stat5* in solution (top) and in thin film (bottom).

All polymers are characterized by an increase in the FWHM of the absorption and fluorescence spectra going from solutions to thin films. For instance, an increase of the absorption band of ~1000 cm^{-1} is observed for AnE-PV*stat*: from 3320 cm^{-1} in solution to 4380 cm^{-1} in thin film. There is a slight bathochromic shift from solution to solid state for the first group (*-stat1, −2, −4, −5*), a hypsochromic shift of the absorption and a bathochromic shift of the emission in the case of *-stat3*, and a red-shift of ~20 nm for the absorption and ~40 nm for the fluorescence in the case of *-stat*. The lowering of the fluorescence quantum yields and lifetimes from solution to thin film is due to additional quenching processes in the thin films.

TABLE 2 Absorption and Emission Data of AnE-PVs in Diluted Chlorobenzene Solution

AnE-PV	λ_a (nm)	λ_f (nm)	Φ_f[a]	$<\tau>$ (ps)[b]	$\Phi_f/<\tau>$ (ns^{-1})	k_{nr} (ns^{-1})[c]
-stat	553	584	0.52	710 ± 10	0.73	0.68
-stat1	504	580	0.14	420 ± 20	0.33	2.1
-stat2	512	583	0.12	380 ± 30	0.32	2.3
-stat3	491	588	0.03	100 ± 10	0.32	9.7
-stat4	513	582	0.18	380 ± 20	0.47	2.2
-stat5	506	581	0.13	350 ± 20	0.37	2.5

[a] ± 10%.
[b] Calculated from biexponential (AnE-PV*stat*) or triexponential (AnE-PV*stat1...5*) fitted decay curves with $<\tau> = 1/(\Sigma_i\Phi_i/\tau_i)$. ϕ_i is the relative yield of the *i*th component: $\Sigma_i\,\phi_i = 1$.
[c] $k_{nr} = (1 - \Phi_f)/<\tau>$.

TABLE 3 Absorption and Emission Data of AnE-PVs in Spin-Casted Films (From Chlorobenzene Solutions)

AnE-PV	λ_a (nm)	λ_f (nm)	Φ_f[a]	$<\tau>$ (ps)[b]	$\Phi_f/<\tau>$ (ns^{-1})	k_{nr} (ns^{-1})[c]
-stat	577	621	0.034	180	0.19	5.4
-stat1	512	613	0.037	79	0.47	12.
-stat2	524	606	0.038	200	0.19	4.8
-stat3	486	618	0.031	100	0.31	9.7
-stat4	523	616	0.022	76	0.29	13
-stat5	510	612	0.033	100	0.33	9.7

[a] ± 0.01.
[b] ± 10 ps. Calculated from triexponential fitted decay curves with $<\tau> = 1 / (\Sigma_i\phi_i/\tau_i)$. ϕ_i is the relative yield of the *i*th component: $\Sigma_i\,\phi_i = 1$.
[c] $k_{nr} = (1 - \Phi_f)/<\tau>$.

Charge Carrier Mobility

In Figure 6, the transfer characteristics in the saturation regime of the OFET devices with different polymers as active layers are presented. The difference in the device performances is rather significant. Drain current variation extends more than two orders of magnitude for the four polymers considered.

In the gradual channel approximation, drain current dependence on the gate voltage can be given by the following equation:

$$I_{ds} = (W/L)\mu(V_{gs})C_i\left[(V_{gs} - V_{th})V_{ds} - 1/2V_{ds}{}^{1/2}\right]$$

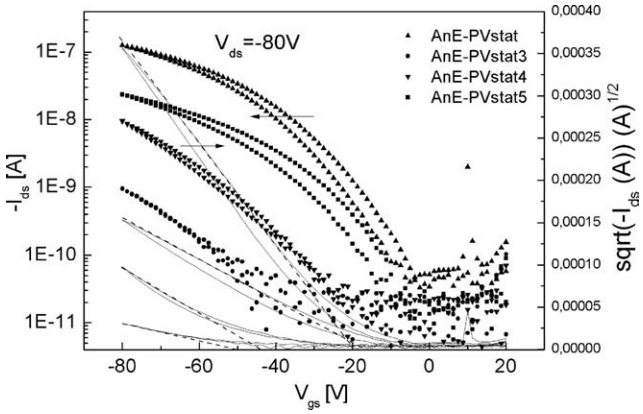

FIGURE 6 Transfer characteristics of the OFET devices with different polymers as active layers. Dashed lines are the linear extrapolation of the square root of the drain currents to determine the threshold voltages.

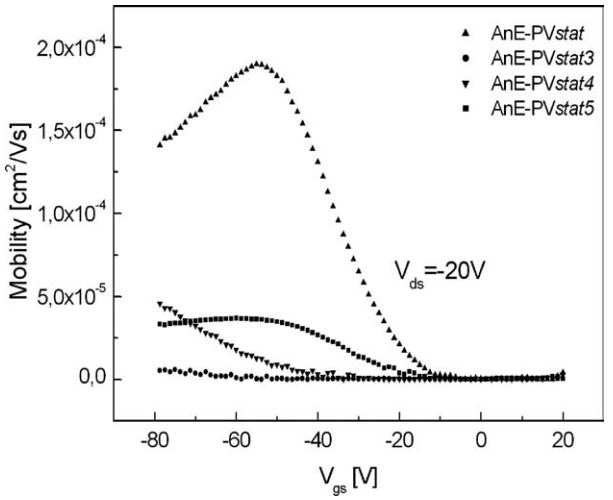

FIGURE 7 Gate voltage-dependent mobilities of the polymers (OFET devices) extracted in the linear regime with the derivation of the drain current.

where I_{ds} is the drain current; μ is the mobility; V_{gs} is the gate voltage; V_{th} is the threshold voltage; W is the channel width, and L is the channel length. The square root of drain current versus gate voltage of the saturation curve can be linearly extended to the "off" current to determine the threshold voltage. Only linear portion of the curves was considered because the mobility is gate voltage dependant as will be discussed later. Threshold voltage is dependent on several factors: such as hole injection barrier between source/drain contact and polymers, total trap density (including dielectric/semiconductor bulk and dielectric/semiconductor interface trap densities), and dielectric capacitance. While dielectric is the same for all the polymers, the large variation in the threshold voltage values can be attributed to the difference in the hole injection barrier coming from the difference in the HOMO levels of the polymers as well as the difference in the interface trap densities. The latter is clearly evidenced in the much higher subthreshold swing of the devices with AnE-PV*stat3* and AnE-PV*stat4*. Dielectric/polymer interface dipole is neglected as PVT has low dielectric constant, and earlier studies showed very low threshold voltages for both n-channel and p-channel devices. Nevertheless, it should be noted that in an OFET structure, most of the device related parameters will be accounted by the threshold voltage. Extracted charge carrier mobility in the linear regime is considered to be more reliable as the distribution of the carriers in the channel is more uniform. Moreover, in a disordered system, charge carrier mobility is strongly dependent on the carrier concentration, that is, the mobility is gate voltage dependent in an OFET device. Taking into account these considerations, gate voltage-dependant mobility of the polymers is shown in Figure 7.

In evaluation of the mobility of the polymers using an OFET structure, contact resistance should be minimized and taken into account, as higher gate voltages will yield underestimated mobility values due to high potential drop at the contacts.[33,34] Staggering configuration does minimize the effect of contact resistance between polymers and source/drain contacts.[35] However, here, we clearly observe the effect of the contact resistance although minimized. In AnE-PV*stat*- and AnE-PV*stat5*-based devices, the super linear increase of the mobility versus gate voltage came to a halt with a maximum. In AnE-PV*stat3* and AnE-PV*stat4* devices, such an effect did not appear, as the effective gate voltage is not high enough due to their rather high threshold voltages. By excluding injection barrier, trap densities and contact resistance, and so forth device-related factors, we can obtain intrinsic mobilities of the polymers through mobility versus effective gate voltage relation in the low gate voltage region as given in Figure 8.

AnE-PV*stat* exhibits the highest mobility ($\sim 10^{-4}$ cm^2 Vs^{-1}) which is almost two orders of magnitude higher than that of AnE-PV*stat3* ($\sim 10^{-6}$ cm^2 Vs^{-1}) and one order of magnitude higher than those of AnE-PV*stat4* and AnE-PV*stat5* ($\sim 10^{-5}$ cm^2 Vs^{-1}). This indicates better interchain stacking ability of the AnE-PV*stat* polymer backbone, as the mobility of the charge carriers strongly depends on the interchain hopping facilitated by π–π stacking. This is consistent with the optical absorption data where AnE-PV*stat* exhibits a clear red-shift and pronounced vibronic feature in the spectrum, whereas AnE-PV*stat3* has obvious blue shift in the absorption maximum comparing to AnE-PV*stat4* and AnE-PV*stat5*. It is also in accord with the scattering results where substantial long-range order is observed in the case of AnE-PV*stat*. One can expect such a large variance in mobilities will eventually lead to rather different performances of these polymers in solar cell devices.

Photovoltaic Studies

Figure 9 shows the thin-film absorption and PL spectra of AnE-PV:PCBM blends. The absorption spectra are rather featureless except of AnE-PV*stat*. AnE-PV*stat* shows a red-shifted absorption feature at around 580 nm. All AnE-PV*stat* samples experience rather strong PL quenching on addition

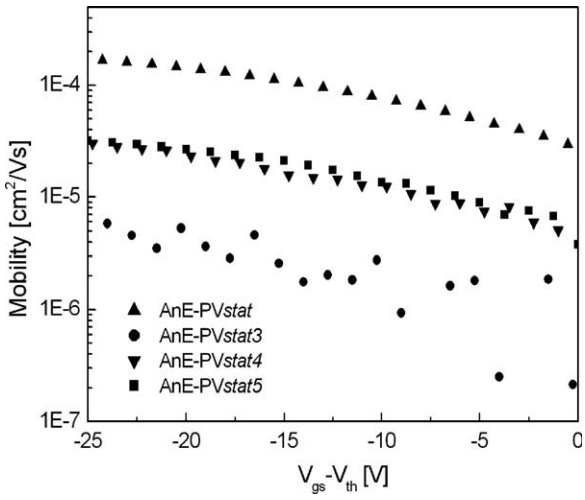

FIGURE 8 Mobility versus effective gate voltage (V_{gs}–V_{th}) of the polymers in the low gate voltage region.

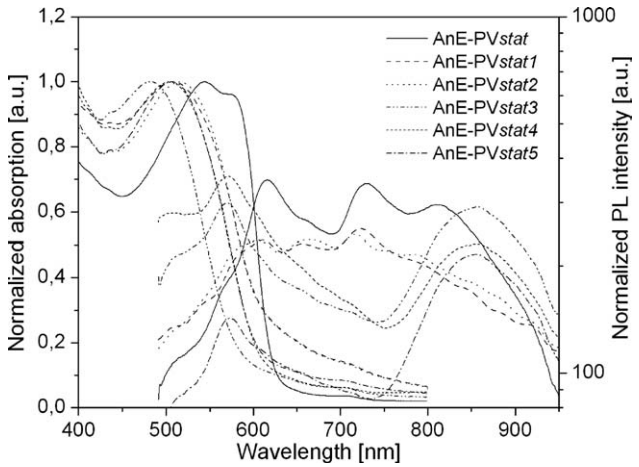

FIGURE 9 Absorption and PL spectra of polymer:PCBM blends spin-coated into thin films.

of PCBM. Quenching factors up to 133 can be observed. Except AnE-PV*stat*, the blended polymer films show no significant features in the PL spectrum. The spectrum of the AnE-PV*stat* sample shows a distinct PCBM feature at around 730 nm that indicates a PCBM-rich phase in the blend films.

A strong tendency toward π–π-stacking in AnE-PV*stat* films is indicated by the pronounced shoulder around 580 nm in the absorption spectrum. The aggregation of the polymer occurs during the film formation from solution. No annealing step was applied. Furthermore, indications for a domain formation in the polymer:PCBM blend arise from the PL spectrum. It shows a pronounced polymer peak around 605 nm and a PCBM peak around 730 nm. Something similar can be observed for AnE-PV*stat*1 and *stat*2 as well. This is a clear sign for a distinct phase separation between polymer and PCBM. While AnE-PV*stat* apparently phase separates and stacks, AnE-PV*stat*1 and *stat*2 seem to show only phase separation but no strong polymer aggregation. Aside the efficient quenching of the polymer PL, effective charge generation and improved charge percolation properties are expected for AnE-PV*stat*:PCBM blends. The other AnE-PVs:PCBM blends should also exhibit a good charge generation; however, a lower charge transport ability that leads to a decrease of the photovoltaic parameters fill factor (FF) and short-circuit current (I_{SC}).

Phase separation is also visible in the AFM topography images. Figure 10 shows the AFM tapping mode images of the polymer:PCBM blends processed into thin films.

AnE-PV*stat*, *stat*1, and *stat*2 show a coarse-grained structure compared to AnE-PV*stat*3, *stat*4, and *stat*5, which have a flat fine-scaled surface morphology. The PCBM blends of AnE-PV*stat*1 and *stat*2 appear more coarse-grained than of AnE-

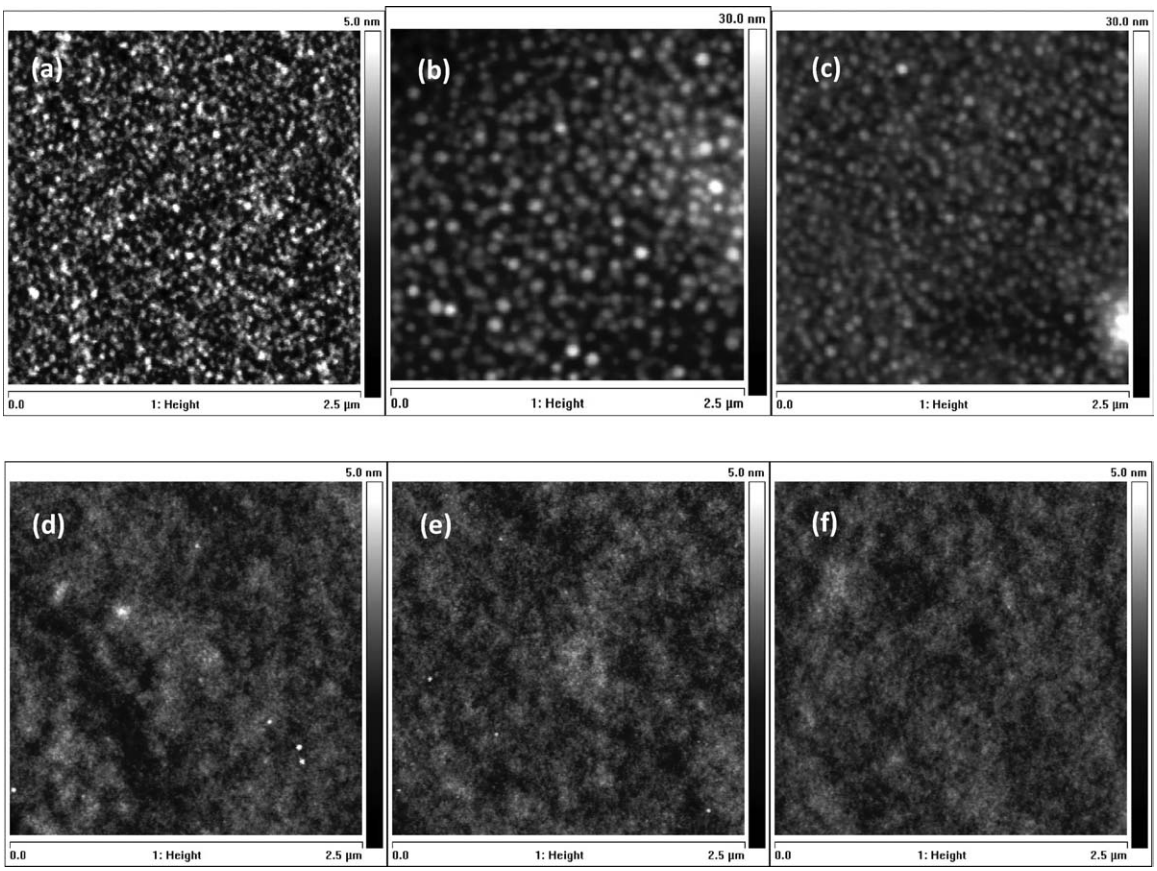

FIGURE 10 AFM topography images of thin films of polymer:PCBM blends: AnE-PV*stat* (a), AnE-PV*stat*1 (b), AnE-PV*stat*2 (c), AnE-PV*stat*3 (d), AnE-PV*stat*4 (e), and AnE-PV*stat*5 (f).

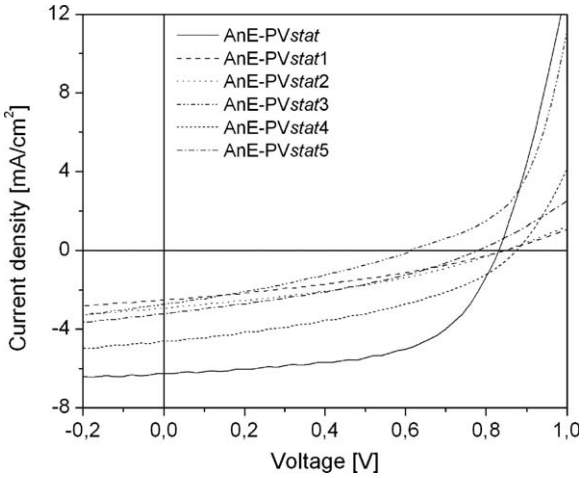

FIGURE 11 *I–V* curves of solar cells utilizing polymer:PCBM blends (1:2 weight ratio).

PV*stat*. Combinations of linear and branched side chains at the polymer backbone seem to induce the formation of coarse-grained structures while the incorporation of asymmetric side-chain-equipped units supports a fine scaled morphology. These observations are in accord with the optical data. The coarse morphology of AnE-PV*stat* is reasonable for the polymer aggregation and phase separation in the blend. Thereby, it can be expected that the AnE-PV*stat*:PCBM blend shows an improved charge percolation due to the pronounced phase separation and π–π-stacking, whereby the fine scale intermixing of the AnE-PV*stat*3, *stat*4, and *stat*5 blends is likely to limit the charge percolation ability impairing their photovoltaic performance. AnE-PV*stat*1 and *stat*2 are expected to show an intermediate percolation ability.

To investigate the photovoltaic performance of the polymers, solar cell devices were fabricated and tested. Figure 11 shows the *I–V* curves of the fabricated solar cells.

In general, for the investigated AnE-PV:PCBM blends, high open-circuit voltages are expected. The highest V_{OC} (872 mV) has been achieved with AnE-PV*stat*4. As expected from the optical and AFM data, AnE-PV*stat* shows the best performance because of efficient charge generation and percolation. Its *I–V* curve exhibits the highest FF and current density. Only the open-circuit voltage is a little bit lower than the one of AnE-PV*stat*4. It is also obvious that the side-chain ratio has no distinct influence on the open-circuit voltage in case of linear and branched side chains. AnE-PV*stat*, *stat*1, and *stat*2 exhibit very similar open-circuit voltage because of similar side-chain volume of linear and branched substitution. The altered side-chain distribution of AnE-PV*stat*1 and *stat*2 dramatically decreases the short-circuit current, FF, and efficiency compared to AnE-PV*stat*. The observed open-circuit voltages for AnE-PV*stat*3, *stat*4, and *stat*5 are in accord with former results. The side-chain volume and the position of the side chains are reasonable for the value of the open-circuit voltage. Table 4 shows the complete set of photovoltaic parameters under AM1.5 illumination for the best solar cell device of each polymer:PCBM blend.

TABLE 4 Photovoltaic Parameters of the Solar Cells Build From Polymer:PCBM Blends (1:2 Weight Ratio)

AnE-PV	I_{sc} (mA cm^{-2})	V_{oc} (mV)	FF (%)	PCE (%)	R_s (Ω)	R_p (Ω)
-*stat*	6.27	828	58.42	3.03	14.6	1,929
-*stat1*	2.52	844	34.03	0.72	75.7	1,295
-*stat2*	2.93	844	35.67	0.88	89	1,120
-*stat3*	2.733	613	31	0.52	8.3	690
-*stat4*	4.628	872	40.89	1.65	15.3	1,091
-*stat5*	3.211	779	34.66	0.87	49.9	837

To further evaluate the photoelectrical behavior, EQE spectra of the best solar cells were recorded. From EQE measurements, there is no percolation problem visible for all polymer:PCBM blends. The signal strength of each polymer clearly correlates to the achieved short-circuit currents. The EQE spectra are shown in Figure 12.

The EQE spectra are in agreement with the absorption properties of the blends (Fig. 9). The feature around 370 nm and the shoulder around 700 nm correspond to the PCBM. The feature size is comparable to the absorption of the blend films. The EQE intensities correlate with the I_{SC} values.

Electroluminescent Properties

To examine the EL properties, single-layer PLEDs were fabricated with AnE-PV*stat*, *stat3*, *stat4*, and *stat5*, respectively, as emissive layer, and LiF and Al as cathode. Polymer LEDs were produced with the configuration: ITO/PEDOT:PSS (50 nm)/AnE-PV (80 nm)/LiF:Al (0.5:100 nm).

EL spectra of all PLEDs are depicted in Figure 13. All devices showed red luminescence (λ_{max} = 608–620 nm). The EL spectra of the polymers were similar to the PL spectra of the

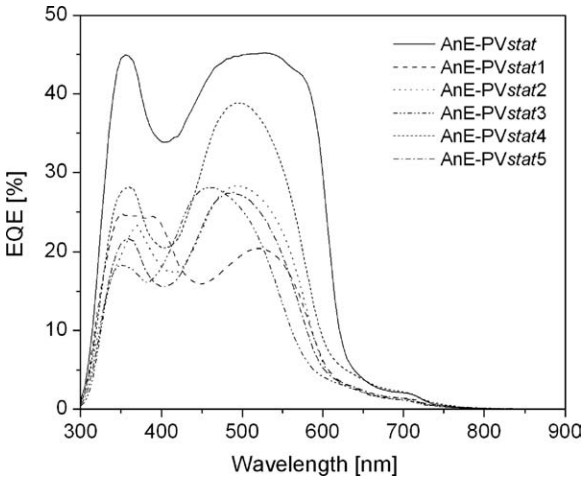

FIGURE 12 EQE spectra of solar cells utilizing polymer:PCBM blends (1:2 weight ratio).

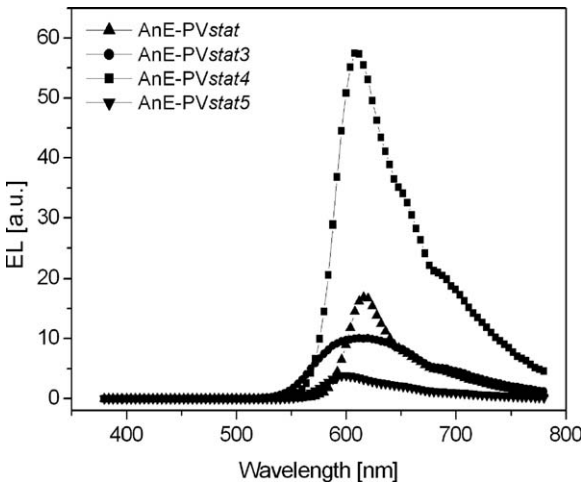

FIGURE 13 EL spectra of ITO/PEDOT:PSS/AnE-PV/LiF:Al devices.

corresponding polymer films. The Commission Internationale d_Eclairage (CIE) chromaticity coordinates 1931 were determined to $(x, y) = (0.66, 0.33)$, (0.59, 0.40), (0.64, 0.35), and (0.61, 0.38) for AnE-PV*stat*, *stat*3, *stat4*, and *stat5*, respectively. These CIE values support the visual impression of red light emission.

Figure 14 shows the current–voltage characteristics of all devices. The current–voltage characteristics of the devices are typical for a diode. The electrical parameters obtained from four devices are summarized in Table 5. CV was used to determine highest occupied molecular orbital (HOMO) and lowest unoccupied molecular orbital (LUMO) levels and electrochemical band gap of AnE-PV*stat*, *stat*3, *stat4*, and *stat5*. Ionization potentials (HOMO levels), $E_{IP,}$ 5.09, 5.14, 5.17, and 5.13 eV were estimated from the corresponding oxidation onset potentials and the electron affinities (LUMO levels), $E_A = 3.04$, 3.02, 3.10, and 3.07 eV were obtained from the onsets of the reduction, and corresponding values of the electrochemical band gap, E_g, were 2.05, 2.12, 2.07, and 2.06 eV for AnE-PV*stat*, AnE-PV*stat3*, AnE-PV*stat4*, and

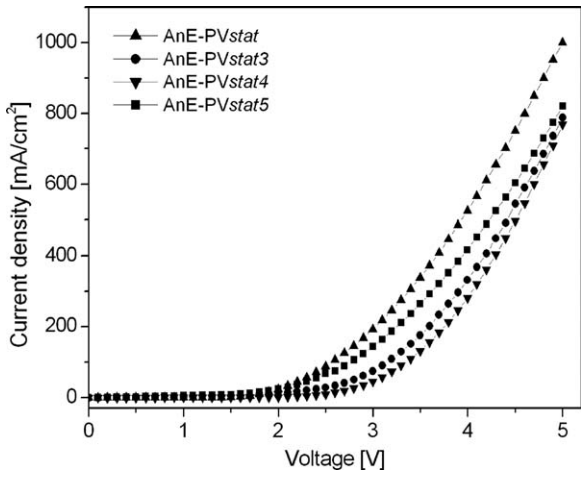

FIGURE 14 Current density–voltage characteristics of ITO/PEDOT:PSS/AnE-PV/LiF:Al devices.

TABLE 5 The Electrical Parameters of PLEDs

Devices	Turn-On Voltage (V)	λ_{EL} (nm)	Maximum Luminance (cd m^{-2})	CIE_x	CIE_y
ITO/PEDOT:PSS/ AnE-PV*stat*/LiF:Al	1.8	616	420	0.66	0.33
ITO/PEDOT:PSS/ AnE-PV*stat3*/LiF:Al	2.0	620	610	0.59	0.40
ITO/PEDOT:PSS/ AnE-PV*stat4*/LiF:Al	1.8	608	2,070	0.64	0.35
ITO/PEDOT:PSS/ AnE-PV*stat5*/LiF:Al	1.8	600	180	0.61	0.38

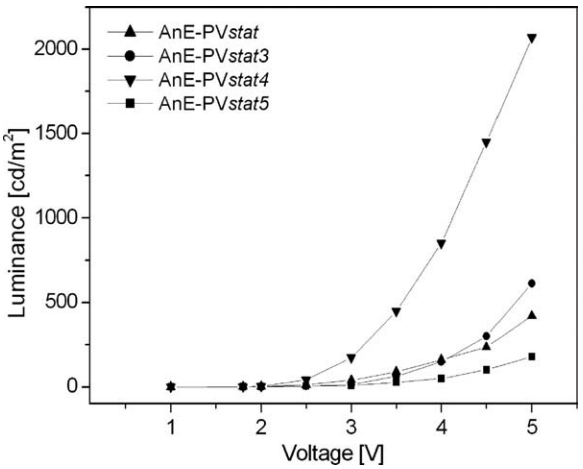

FIGURE 15 Luminance–voltage characteristics of ITO/PEDOT:PSS/AnE-PV/LiF:Al devices.

AnE-PV*stat5*, respectively. Because of the low ionization potential of these polymers, all devices exhibit a low turn-on voltage (taken as the voltage at which the luminance exceeds 1 cd m^{-2}) of ~2 V. The high resemblance of the turn-on voltage of the PLEDs can be further explained by the almost identical HOMO levels of the polymers, which leads to similar hole injection barriers between PEDOT:PSS layer and polymer layer in all devices.

The luminance–voltage characteristics of devices are shown in Figure 15. Polymer LED with AnE-PV*stat4* active layer showed a maximum luminance of 2070 cd m^{-2} at 5 V. Polymer AnE-PV*stat4* has linear octyloxy, asymmetric substitution with methyloxy, and 2-ethylhexyloxy side chains, and it has lower amount of branched side chain than the other polymers (AnE-PV*stat*, *stat*3, and *stat5*). The size of the side chain can have a dramatic effect on the EL performance.[25] It should be pointed out that the EL performance of the AnE-PVs is strongly dependent on the nature and distribution of the attached side chains.

CONCLUSIONS

Anthracene-containing PPE-PPV copolymers with various statistical side-chain distributions were studied. Charge carrier mobilities in thin films of these polymers were investigated

using OFET. Taking into account all device-related parameters, intrinsic mobilities of the polymers were derived exhibiting rather large variances, falling in the range of almost two orders of magnitude, indicating rather different π–π stacking behavior of the polymer backbones. Solar cells fabricated from these polymers were found to show quite different photovoltaic behavior. While AnE-PV*stat* shows a strong tendency of aggregation when processed from solution and therefore high π–π-stacking ability, the other polymers appear less suitable for photovoltaic application. The strong exciton quenching of all polymers on blending with PCBM is promising for photovoltaic applications, but only for AnE-PV*stat*, this leads to efficient photovoltaic devices. The incorporation of elements with asymmetric methoxy/ethylhexyloxy side-chain attachments into the copolymer seems to decrease the overall solar cell performance. Polymer AnE-PV*stat3* without any linear octyloxy side-chain components showed the worst photovoltaic performance. Polymer LEDs were fabricated using a selection of four polymers. All devices showed low turn-on voltage of $\sim$2 V and exhibited red light emission with maxima between 608 and 620 nm. The device containing AnE-PV*stat4* as active layer showed a maximum luminance of 2070 cd m^{-2} at 5 V.

ACKNOWLEDGMENTS

D. A. M. Egbe, H. Hoppe, and S. Rathgeber are grateful to the Deutsche Forschungsgemeinschaft (DFG) for financial support in the framework of SPP1355. O. Usluer and N. S. Sariciftci thank the European Science Foundation (Research Networking Program "New Generation of Organic based Photovoltaic Devices" ORGANISOLAR). V. Cimrova acknowledges the support of the Ministry of Education, Youth and Sports of the Czech Republic (grant N° 1M06031).

REFERENCES AND NOTES

1 Sariciftci, N. S.; Smilowitz, L.; Heeger, A. J.; Wudl, F. *Science* **1992,** *258*, 1474–1476.

2 (a) Hoppe, H.; Sariciftci, N. S. *Adv. Polym. Sci.* **2008,** *214*, 1–86; (b) Günes, S.; Neugebauer, H.; Sariciftci, N. S. *Chem. Rev.* **2007,** *107*, 1324–1338; (c) Dennler, G.; Lungenschmied, C.; Neugebauer, H.; Sariciftci, N. S.; Labouret, A. *J. Mater. Res.* **2005,** *20*, 3224–3233; (d) Cheng, Y.-J.; Yang, S.-H.; Hsu, C.-S. *Chem. Rev.* **2009,** *109*, 5868–5923.

3 (a) Brabec, C. J.; Hauch, J. A.; Schilinsky, P.; Waldauf, C. *MRS Bull.* **2005,** *30*, 50–52; (b) Li, G.; Shotriya, V.; Huang, J.; Yao, Y.; Moriarty, T.; Emery, K.; Yang, Y. *Nat. Mater.* **2005,** *4*, 864–868.

4 (a) Ma, W.; Yang, C.; Gong, X.; Lee, K.; Heeger, A. *J. Adv. Funct. Mater.* **2005,** *15*, 1617–1622; (b) Reyes-Reyes, M.; Kim, K.; Carolla, D. L. *Appl. Phys. Lett.* **2005,** *87*, 083506–083508.

5 McCulloch, I.; Heeney, M.; Chabinyc, M. L.; DeLongchamp, D.; Kline, R. J.; Cölle, M.; Duffy, W.; Fischer, D.; Gundlach, D.; Hamadani, B.; Hamilton, R.; Richter, L.; Salleo, A.; Shkunov, M.; Sparrowe, D.; Tierney, S.; Zhang, W. *Adv. Mater.* **2009,** *21*, 1091–1109.

6 (a) Kim, J. Y.; Lee, K.; Coates, N. S.; Moses, D.; Nguyen, T. Q.; Dante, M.; Heeger, A. *J. Sci.* **2007,** *317*, 222–225; (b) Park, S. H.; Roy, A.; Beaupre, S.; Cho, S.; Coates, N.; Moon, J. S.; Moses, D.; Leclerc, M.; Lee, K.; Heeger, A. *J. Nat. Photon.* **2009,** *3*, 297–302; (c) Chen, H.-Y.; Hou, J.; Zhang, S.; Liang, Y.; Yang, G.; Yang, Y.; Yu, L.; Wu, Y.; Li, G. *Nat. Photon.* **2009,** *3*, 649–653; (d) Liang, Y.; Feng, D.; Wu, Y.; Tsai, S.-T.; Li, G.; Ray, C.; Yu, L. *J. Am. Chem. Soc.* **2009,** *131*, 7792–7799.

7 Service, R. *Science* **2011,** *332*, 293.

8 http://www.photovoltaik4all.de (accessed July 1, 2011).

9 (a) Yao, Y.; Hou, J.; Xu, Z.; Li, G.; Yang, Y. *Adv. Funct. Mater.* **2008,** *18*, 1783–1789; (b) Chen, L.; Hong, Z.; Li, G.; Yang, Y. *Adv. Mater.* **2009,** *21*, 1434–1449.

10 Egbe, D. A. M.; Türk, S.; Rathgeber, S.; Kühnlenz, F.; Jadhav, R.; Wild, A.; Birckner, E.; Adam, G.; Pivrikas, A.; Cimrova, V.; Knör, G.; Sariciftci, N. S.; Hoppe, H. *Macromolecules* **2010,** *43*, 1261–1269.

11 Rathgeber, S.; de Toledo, D. B.; Birckner, E.; Hoppe, H.; Egbe, D. A. M. *Macromolecules* **2010,** *43*, 306–315.

12 Egbe, D. A. M.; Adam, G.; Pivrikas, A.; Ramil, A. M.; Birckner, E.; Cimrova, V.; Hoppe, H.; Sariciftci, N. S. *J. Mater. Chem.* **2010,** *20*, 9726–9734.

13 (a) Egbe, D. A. M.; Ulbricht, C.; Orgis, T.; Carbonnier, B.; Kietzke, T.; Peip, M.; Metzner, M.; Gericke, M.; Birckner, E.; Pakula, T.; Neher, D.; Grummt, U.-W. *Chem. Mater.* **2005,** *17*, 6022–6032; (b) Egbe, D. A. M.; Roll, C. P.; Birckner, E.; Grummt, U.-W.; Stockmann, R.; Klemm, E. *Macromolecules* **2002,** *35*, 3825–3837.

14 Kim, D. W.; Kim, H.-K.; Son, J.-M.; Kee, I.-S.; Hwang, D.-H.; Chung, M.-C.; Lee, J.-H.; *J. Lumin.* **2011,** *131*, 1288–1293.

15 Friend, R. H.; Gymer, R. W.; Holmes, A. B.; Burroughes, J. H.; Marks, R. N.; Taliani, C.; Bradley, D. D. C.; Dos Santos, D. A.; Brédas, J. L.; Lögdlund, M.; Salaneck, W. R. *Nature* **1999,** *397*, 121–128.

16 Baek, N. S.; Kim, H. K.; Chae, E. H.; Kim, B. H.; Lee, J. H. *Macromolecules* **2002,** *35*, 9282–9288.

17 Li, S.; Zhao, P.; Huang, Y.; Li, T.; Tang, C.; Zhu, R.; Zhao, L.; Fan, Q.; Huang, S.; Xu, Z.; Huang, W. *J. Polym. Chem. Part A: Polym. Chem.* **2009,** *47*, 2500–2508.

18 Kang, J. M.; Cho, H. J.; Lee, J.; Lee, J. I.; Lee, S. K.; Cho, N. S.; Hwang, D. H.; Shim, S. K. *Macromolecules* **2006,** *39*, 4999–5008.

19 Berggren, M.; Inganas, O.; Gustafsson, G.; Rasmusson, J.; Andersson, M. R.; Hjertberg, T.; Wennerstrom, O. *Nature* **1994,** *372*, 444–446.

20 Remmers, M.; Neher, D.; Grüner, J.; Friend, R.-H.; Gelinck, G. H.; Warman, J. M.; Quattrocchi, C.; Dos Santos, D. A.; Bredas, J. L. *Macromolecules* **1996,** *29*, 7432–7445.

21 Yi, H.; Iraqi, A.; Stevenson, M.; Elliott, C. J.; Lidzey, D. G. *Macromol. Rapid Commun.* **2007,** *28*, 1155–1160.

22 Lu, S.; Liu, T.; Ke, L.; Ma, D.-G.; Chua, S.-J.; Huang, W. *Macromolecules* **2005,** *38*, 8494–8502.

23 Wu, C. W.; Tsai, C. M.; Lin, H. C. *Macromolecules* **2006,** *39*, 4298–4305.

24 Peng, Z.; Zhang, J.; Xu, B. *Macromolecules* **1999,** *32*, 5162–5164.

25 Grimsdale, A. C.; Chan, K. L.; Martin, R. E.; Jokisz, P. G.; Holmes, A. B. *Chem. Rev.* **2009,** *109*, 897–1091.

26 Tada, K.; Onoda, M.; Hirohata, M.; Kawai, T.; Yoshino, K. *Jpn. J. Appl. Phys. Part 2* **1996,** *35*, L251–L253.

27 Hirohata, M.; Tada, K.; Kawai, T.; Onoda, M.; Yoshino, K. *Synth. Met.* **1997,** *85*, 1273–1274.

28 Lu, S. L.; Yang, M. J.; Luo, J.; Cao, Y.; Bai, F. L. *Synth. Met.* **2004,** *146*, 175–180.

29 Sun, J.; Chen, J.; Zou, J.; Ren, S.; Zhong, H.; Zeng, D.; Du, J.; Xu, E.; Fang, Q. *Polymer* **2008,** *49*, 2282–2287.

30 Park, J.-W.; Kang, P.; Park, H.; Oh, H.-Y.; Yang, J.-H.; Kim, Y.-H.; Kwon, S.-K. *Dyes Pigment* **2010,** *85*, 93–98.

31 Abbas, M.; Cakmak, G.; Tekin, N.; Kara, A.; Guney, H. Y.; Arici, E.; Sariciftci, N. S. *Org. Electron.* **2011,** *12*, 497–503.

32 (a) Wild, A.; Egbe, D. A. M.; Birckner, E.; Cimrova, V.; Baumann, R.; Grummt, U.-W.; Schubert, U. S. *J. Polym. Sci. Part A: Polym. Chem.* **2009,** *47*, 2243–2261; (b) Hoppe, H.; Egbe, D. A. M.; Mühlbacher, D.; Sariciftci, N. S. *J. Mater. Chem.* **2004,** *14*, 3462–3467; (c) Egbe, D. A. M.; Bader, C.; Nowotny, J.; Günther, W.; Klemm, E. *Macromolecules* **2003,** *36*, 5459–5469.

33 Mansouria, S.; Horowitz, G.; Bourguiga, R. *Synth. Met.* **2010,** *160*, 1787–1792.

34 Horowitz, G.; Hajlaoui, R.; Fichou, D.; El Kassmi, A. *J. Appl. Phys.* **1999,** *85*, 3202–3206.

35 Street, R. A.; Salleo, A. *Appl. Phys. Lett.* **2002,** *81*, 2887–2889.